An Approach to Multimodal Biomedical Image Registration Utilizing Particle Swarm Optimization

Mark P. Wachowiak, *Member, IEEE*, Renata Smolíková, *Member, IEEE*, Yufeng Zheng, Jacek M. Zurada, *Fellow, IEEE*, and Adel S. Elmaghraby, *Senior Member, IEEE*

***Abstract*—Biomedical image registration, or geometric alignment of two-dimensional and/or three-dimensional (3-D) image data, is becoming increasingly important in diagnosis, treatment planning, functional studies, computer-guided therapies, and in biomedical research. Registration based on intensity values usually requires optimization of some similarity metric between the images. Local optimization techniques frequently fail because functions of these metrics with respect to transformation parameters are generally nonconvex and irregular and, therefore, global methods are often required. In this paper, a new evolutionary approach, particle swarm optimization, is adapted for single-slice 3-D-to-3-D biomedical image registration. A new hybrid particle swarm technique is proposed that incorporates initial user guidance. Multimodal registrations with initial orientations far from the ground truth were performed on three volumes from different modalities. Results of optimizing the normalized mutual information similarity metric were compared with various evolutionary strategies. The hybrid particle swarm technique produced more accurate registrations than the evolutionary strategies in many cases, with comparable convergence. These results demonstrate that particle swarm approaches, along with evolutionary techniques and local methods, are useful in image registration, and emphasize the need for hybrid approaches for difficult registration problems.**

***Index Terms*—Evolutionary strategies, global optimization, image registration, local optimization, particle swarm optimization.**

I. Introduction

MEDICAL imaging provides insights into the size, shape, and spatial relationships among anatomical structures. For instance, computer-assisted tomography (CT) is very useful for imaging bony structures and dense tissue, whereas magnetic resonance imaging (MRI) and ultrasound (US) provide views of soft tissues. Additionally, functional imaging is becoming increasingly important both clinically and in medical research. For example, positron emission tomography (PET) and single-photon computed tomography (SPECT) imaging provide information on blood flow and metabolic processes. Very often, areas of the body are imaged with different modalities. These images are used in a complimentary manner to gain additional insights into a phenomenon.

For these different modalities to be useful, they must be appropriately combined, or *fused*. Before images can be fused, they must first be geometrically and/or temporally aligned. This alignment process is known as *registration*. One of the most important applications of registration is image-guided therapy, and registration in neurosurgery and orthopaedic surgery is now common [1]. Registration is also used in treatment planning [2]–[4], in functional brain imaging [2], [3], [5], and in brain atlases and mapping [2]. Developing applications include multimedia patient records [1], postgenomic registration to characterize gene function [1], registration of intra- and preoperative images in surgical interventions [1], and treatment monitoring [2].

There are many approaches to biomedical image registration. The "gold standard" utilizes markers placed on the subject [2], [3]. Other approaches include matching extracted features or surfaces [2]. Much work has recently focused on *intensity-based* approaches, in which the intensity values (color, or gray level) are used to compute similarity measures between the images. Such metrics are called voxel (volume element) measures. Intensity-based registration does not generally require extensive preprocessing, such as segmentation or feature extraction. In intensity-based registration, there are generally three important considerations [3], [6].

1) The *search space* is the class of potential transformations, such as rigid body and elastic, used to align the images. Three-dimensional (3-D) rigid-body registration has six degrees of freedom: x, y, and z translations (denoted as t_x, t_y, and t_z, respectively), and rotations about the x, y, and z axes (respectively, denoted as α, β, and γ). The addition of shearing and scaling results in an affine transformation. The most general class of transformations, nonlinear registrations includes nonlinear mapping functions (e.g., polynomials), where curved lines are mapped onto other curved lines.
2) The *similarity metric* is an indicator of how closely the features or intensity values of two images match. The sum of squared intensity difference [7], generalized correlation coefficient [8], ratio image uniformity [7], and information theoretic measures [2], [3], [9]–[11] are commonly used similarity measures.

Manuscript received July 10, 2002; revised November 15, 2003. The work J. M. Zurada was supported in part by the Systems Research Institute, Polish Academy of Science, Warsaw, Poland.

M. P. Wachowiak and R. Smolíková were with the Department of Computer Engineering and Computer Science, University of Louisville, Louisville, KY 40292 USA. They are now with Imaging Research Laboratories, Robarts Research Institute, London, ON N6A 5K8, Canada (e-mail: mwach@imaging.robarts.ca; smolikov@imaging.robarts.ca).

Y. Zheng and A. S. Elmaghraby are with the Department of Computer Engineering and Computer Science, University of Louisville, Louisville, KY 40292 USA (e-mail: yufeng.zheng@uofl.edu; adel@louisville.edu).

J. M. Zurada is with the Department of Electrical and Computer Engineering, University of Louisville, Louisville, KY 40292 USA (e-mail: jmzura02@athena.louisville.edu).

Digital Object Identifier 10.1109/TEVC.2004.826068

3) The *search strategy* optimizes the similarity metric. Examples include local or global searches, multiresolution approaches or other optimization techniques.

The focus of the current paper is the search strategy (optimization) for maximizing the similarity metric for registering single slice biomedical images to 3-D volumes, where the images were obtained from different modalities. Single slice to 3-D registration is useful in such areas as image-guidance during interventional procedures. It is challenging because of the low amount of data from which to compute the similarity metric. In addition, registration of two-dimensional (2-D) modalities (e.g., X-ray scans) to 3-D tomographic data is a rapidly developing research area. Specifically, *particle swarm optimization* (PSO) is proposed as a global optimization approach for biomedical image registration. To the authors' knowledge, PSO has not yet been applied to registration. PSO is a paradigm that includes many variations, and in this paper, several such variants are employed. Additionally, a new PSO approach specifically tailored to the image registration problem is proposed. This method makes use of the initial user-specified orientation of the images to be registered. In practice, registration success is heavily dependent on the initial orientation before any optimization is applied [2], [3], [7]. The proposed PSO technique assumes this orientaion to be "in the general vicinity" of the correct transformation, and also employs local optimization.

The paper is organized as follows. First, the registration problem is formulated. Following is a brief discussion of similarity metrics and of other optimization techniques. Next, adaptation of PSO to image registration is described, and the proposed PSO improvement for registration is presented. Experiments to test the new algorithm are described in the next section. The results are compared with seven evolutionary strategies. Performance analysis, including accuracy and efficiency, is then given, and a discussion of the results concludes the paper.

II. Image Registration Process

In the discussion that follows, it is assumed that an "image" can have two or three dimensions. Let $\mathbf{T}$ denote the spatial transformation that maps features or coordinates (spatial locations) from one image or coordinate space to another image or coordinate space. Let $\mathbf{p}_A$ and $\mathbf{p}_B$ denote coordinate points (pixel locations) in images A and B, respectively. The image registration problem is to determine $\mathbf{T}$ so that the mapping $\mathbf{T}$: $\mathbf{p}_A \rightarrow \mathbf{p}_B \Leftrightarrow \mathbf{T}(\mathbf{p}_A) = \mathbf{p}_B$ results in the "best" alignment of A and B [2]. For 3-D rigid body registration, the mapping of coordinates $\mathbf{p} = [x\ y\ z]^{\mathrm{T}}$ into $\mathbf{p}' = [x'\ y'\ z']^{\mathrm{T}}$ can be formulated as a matrix multiplication in homogeneous coordinates [7], as shown in (1) at the bottom of the page. Because digital images are sampled on a discrete grid, but $\mathbf{T}$ generally maps to continuous values, interpolation of intensities is required [2].

Although elastic transformations are more realistic (as most body tissues are deformable to some degree), rigid body registration is generally performed to initially determine global alignment, followed by local elastic registration [12]. Furthermore, many nonlinear registration methods align small blocks of the floating image to the reference image in a linear manner [13], [14]. Thus, because of its wide applicability, and to demonstrate the efficacy of using PSO methods in registration, rigid body transformations are considered in the current study. That is, the goal of the optimization is to determine the parameters t_x, t_y, t_z, α, β, and γ.

A. Similarity Metric (Objective Function)

Similarity metrics for image registration must be robust; that is, they should attain a global maximum (or a very distinct local maximum) at the correct registration. The "best registration" is very often a local (not global) optimum [2], [7]. Thus, in addition to exercising care when selecting an initial orientation [7], other features, such as intensity gradient information, should also be utilized [15]. However, in this paper, it is assumed that the global optimum is attained at the correct registration transformation.

Much of the current work on biomedical image registration utilizes information theoretic voxel similarity measures, in particular, mutual information based on the Shannon definition of entropy [9], [10]. Mutual information has been shown to be robust for multimodal registration, and does not depend on the specific dynamic range or intensity scaling of the images. It is a measure of the relative independence of two images [7]. High values indicate high dependence. The mutual information of two images A and B is given as

$$I(A,B) = H(A) + H(B) - H(A,B) \tag{2}$$

where H denotes Shannon entropy. For an image A with N pixels and with each intensity value $i = 1, \ldots N$, occurring with frequency p_i, the Shannon entropy is computed as

$$H(A) = -\frac{1}{N}\sum_{i=1}^{N} p_i \log p_i. \tag{3}$$

For each intensity, the p_i can be estimated with Parzen windows [10], histograms, or other probability density estimators.

$$\begin{bmatrix} \mathbf{p}' \\ 1 \end{bmatrix} = \mathbf{T} \begin{bmatrix} \mathbf{p} \\ 1 \end{bmatrix} \Leftrightarrow$$
$$\begin{bmatrix} x' \\ y' \\ z' \\ 1 \end{bmatrix} = \begin{bmatrix} \cos\beta\cos\gamma & \cos\alpha\sin\gamma + \sin\alpha\sin\beta\cos\gamma & \sin\alpha\sin\gamma - \cos\alpha\sin\beta\cos\gamma & t_x \\ -\cos\beta\sin\gamma & \cos\alpha\cos\gamma - \sin\alpha\sin\beta\sin\gamma & \sin\alpha\cos\gamma + \cos\alpha\sin\beta\sin\gamma & t_y \\ \sin\beta & -\sin\alpha\cos\beta & \cos\alpha\cos\beta & t_z \\ 0 & 0 & 0 & 1 \end{bmatrix} \begin{bmatrix} x \\ y \\ z \\ 1 \end{bmatrix} \tag{1}$$

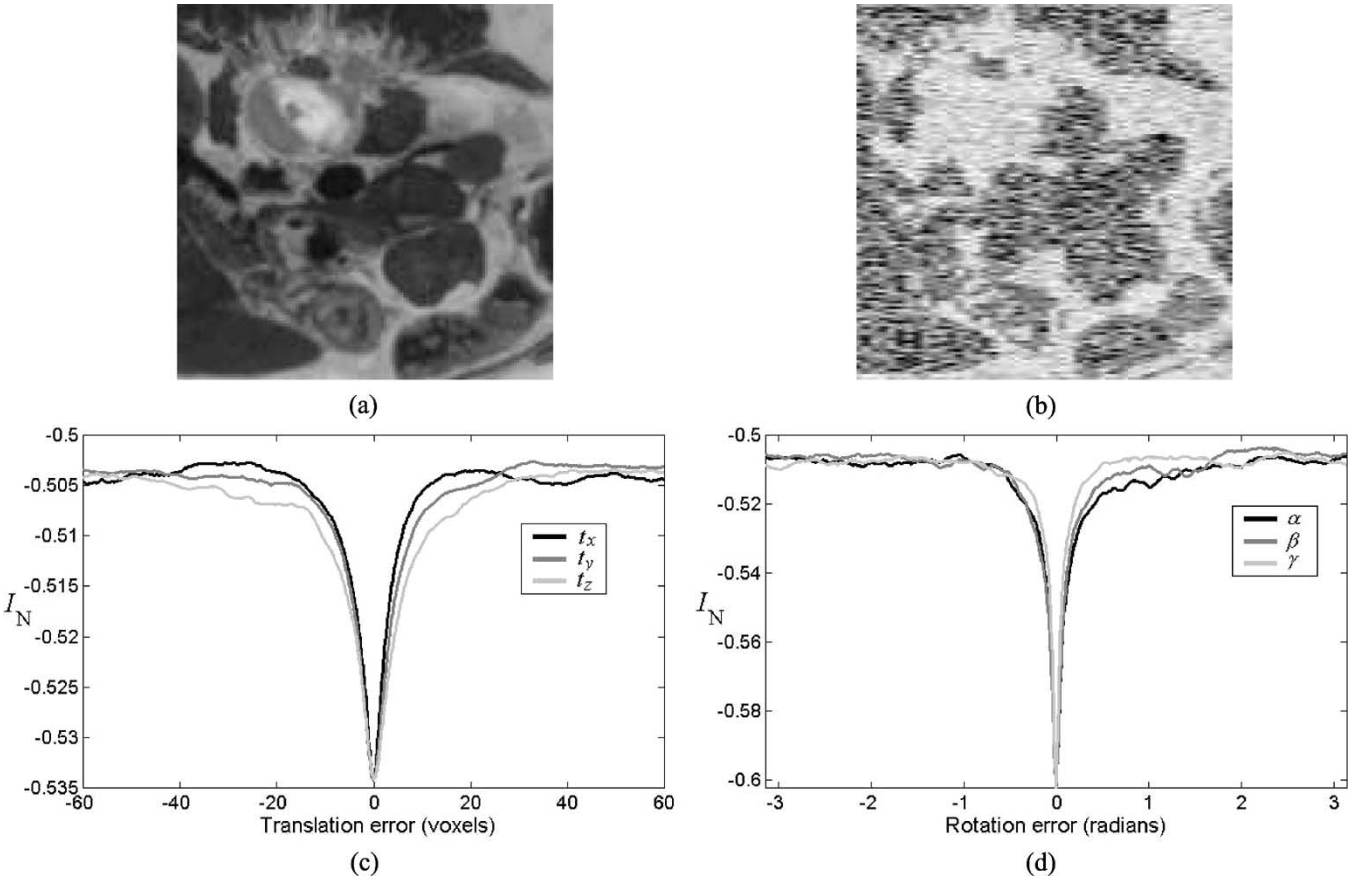

Fig. 1. (a) Slice from abdominal histological volume. (b) Corresponding simulated US image. (c) Normalized mutual information as a function of translation errors. (d) Normalized mutual information as a function of rotation errors.

$H(A, B)$ is computed with an estimate of the joint density. Normalized mutual information I_N, given as

$$I_N(A, B) = \frac{H(A) + H(B)}{2H(A, B)} \tag{4}$$

is less sensitive to the size of the partal overlap between the 2-D image and the volume [11]. As optimization in image registration is to maximize similarity, similarity metric values, as functions of transformation parameters, comprise the objective function, henceforth denoted as $f(\mathbf{x})$. Many optimization problems are formulated as minimization problems and, thus, without loss of generality, it is understood that for image registration, the goal is to minimize $-f(\mathbf{x})$. Figs. 1–3 show slices from 3-D volumes, 2-D images to be registered with these volumes, and $-I_N$ for $t_x, t_y, t_z, \alpha, \beta$, and γ misalignments. For each curve, consisting of 1000 misregistrations, a single parameter was varied, while the other five parameters were held constant. Although the minimum values are well-defined, the functions are not smooth, and are characterized by many local minima, particularly evident in Fig. 1(c). Also, the effect of gray level interpolation is demonstrated in Fig. 2(c) by the ripples in the curve.

The success of registration algorithms also depends on the similarity metric. Although there is yet no proof for the optimality of information-theoretic measures [2], because of its robustness and good results in previous studies [2], [7], [13], normalized mutual information was selected as the similarity measure in the current study. This metric is robust, in the sense that it usually attains its maximum at correct alignment, but is still generally nonsmooth and prone to local optima, as is the case with other metrics. For this reason, global optimization approaches are warranted.

B. Optimization of Similarity Metrics

Local methods, such as Powell's direction set method [16], [17], conjugate gradient [17], Levenberg–Marquardt [17], or the Nelder–Mead simplex algorithm [16], [17], are generally used in image registration. Because many similarity metrics, as functions of transformation parameters, are generally irregular and rough (especially for multimodal registration), local methods are most accurate when the initial orientation is very close to the transformation that yields the best registration.

One approach to address this issue is to apply multiresolution techniques, whereby images are registered at increasing resolutions with initial orientations from the preceding (lower) resolution [16], [18]. These methods still frequently become trapped in local optima, as the global optimum may not be present in lower resolutions [2], [19]. Therefore, global optimization is often required. Such global approaches include simulated annealing [20], genetic algorithms [20], [21], evolutionary strategies [19], [22], and the tabu search [23]. In registration, evaluating (4) can be very costly, as joint density estimation and interpolation are all involved. Therefore, the number of objective function evaluations must be as low as

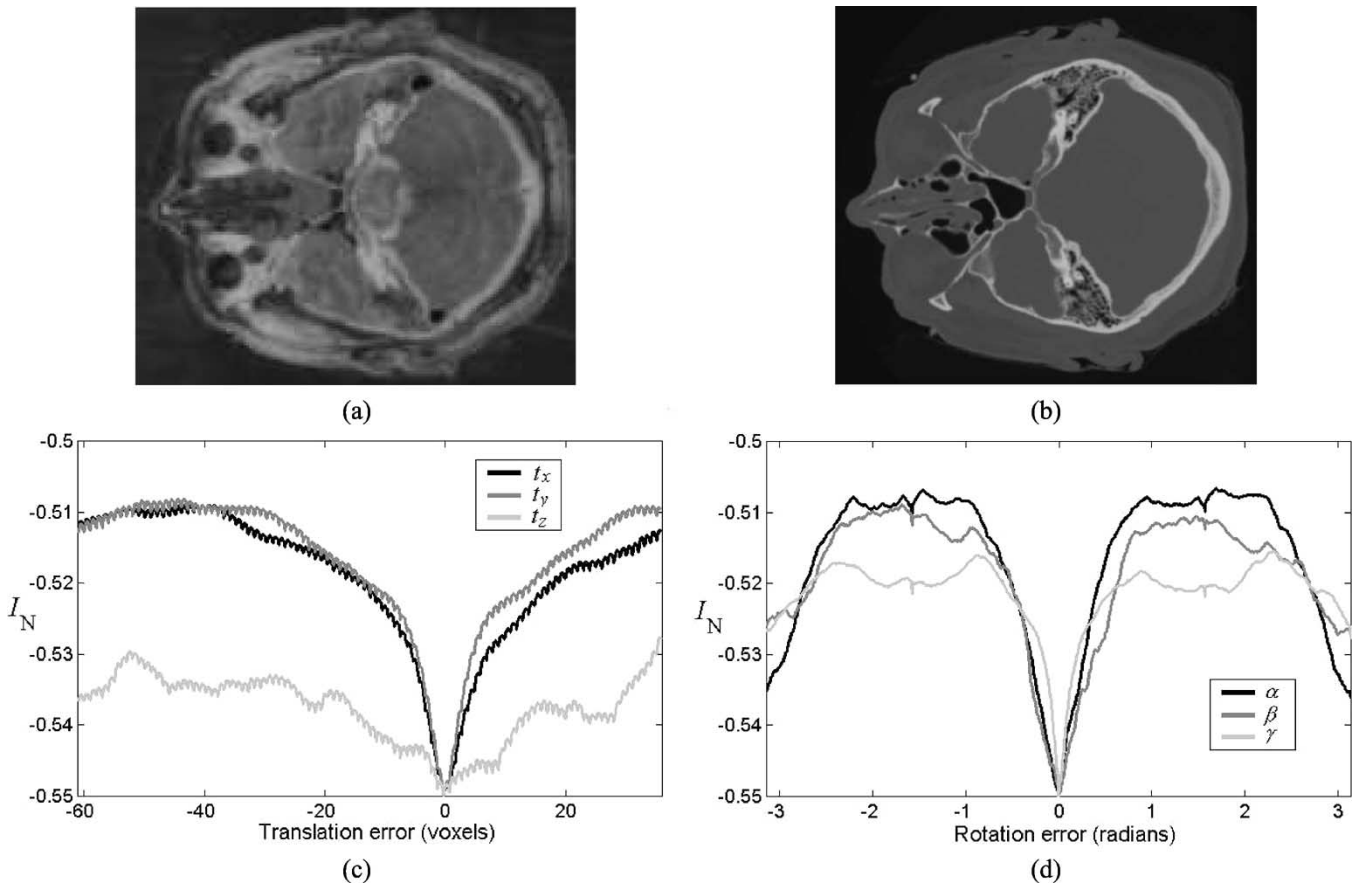

Fig. 2. (a) Slice from head histological volume. (b) Corresponding CT image. (c) Normalized mutual information as a function of translation errors. (d) Normalized mutual information as a function of rotation errors.

possible. Efficiency is the primary reason that local techniques are preferred for registration. However, efficient global optimization may gain acceptance if a marked improvement in accuracy can be demonstrated [19]–[23].

III. Image Registration Using PSO

PSO is a relatively new population-based evolutionary computation technique [24], [25]. In contrast to genetic algorithms (GAs) and evolutionary strategies (ESs,) which exploit the competitive characteristics of biological evolution (e.g., survival of the fittest), PSO exploits cooperative and social aspects, such as fish schooling, birds flocking, and insects swarming. Starting from a diffuse population, now called a swarm, individuals, now termed as particles, tend to move about the search space, eventually clustering in regions where minima are identified. Investigation into the theoretical properties of PSO is an active research area [25]–[27]. Practical applications of PSO have also appeared, including NC programming [28], process biochemistry [29], optimizing power flow [30], neural network training [25], and tremor analysis [25].

In PSO, at each iteration, the ith particle $\mathbf{x}_i$, $i = 1, \ldots, N$, (N is the number of particles) moves by addition of a velocity vector $\mathbf{v}_i$, which is a function of the best position (the position attaining the lowest objective function value) found by that particle, ($\mathbf{p}_i$, for personal best) and of the best position found so far among all particles ($\mathbf{g}$, for global best). $\mathbf{x}_i$, $\mathbf{v}_i$, $\mathbf{p}_i$, and $\mathbf{g}$ are D-dimensional vectors. At iteration t, the position of the ith particle is given as [25]

$$\begin{cases} \mathbf{v}_i(t) = w(t)\mathbf{v}_i(t-1) + \varphi_1 u_1 (\mathbf{p}_i - \mathbf{x}_i(t-1)) \\ \qquad\qquad + \varphi_2 u_2 (\mathbf{g} - \mathbf{x}_i(t-1)) \\ \mathbf{x}_i(t+1) = \mathbf{x}_i(t) + \mathbf{v}_i(t) \end{cases} \tag{5}$$

where $w(t)$ is the *inertial weight*, the φ are *acceleration constants*, and the $u \in (0,1)$ are uniformly distributed random numbers. To keep the $\mathbf{x}_i$ within reasonable bounds, velocities are often clamped to a maximum velocity $\mathbf{v}_{\max}$: $\mathbf{v}_i \in [-\mathbf{v}_{\max}, \mathbf{v}_{\max}]$. (Full implementation details are found in [25].)

The performance of PSO is dependent on the parameter settings: inertial weights $w(t)$, acceleration constants φ, the maximum number of iterations T, and the initialization of the population. The inertial weight w is usually a monotonically decreasing function of the iteration t. For example, given a user-specified maximum weight $w_{\max}$ and a minimum weight $w_{\min}$, one way to update w is as follows:

$$w(t+1) = w(t) + dw, \quad dw = \frac{(w_{\min} - w_{\max})}{T}. \tag{6}$$

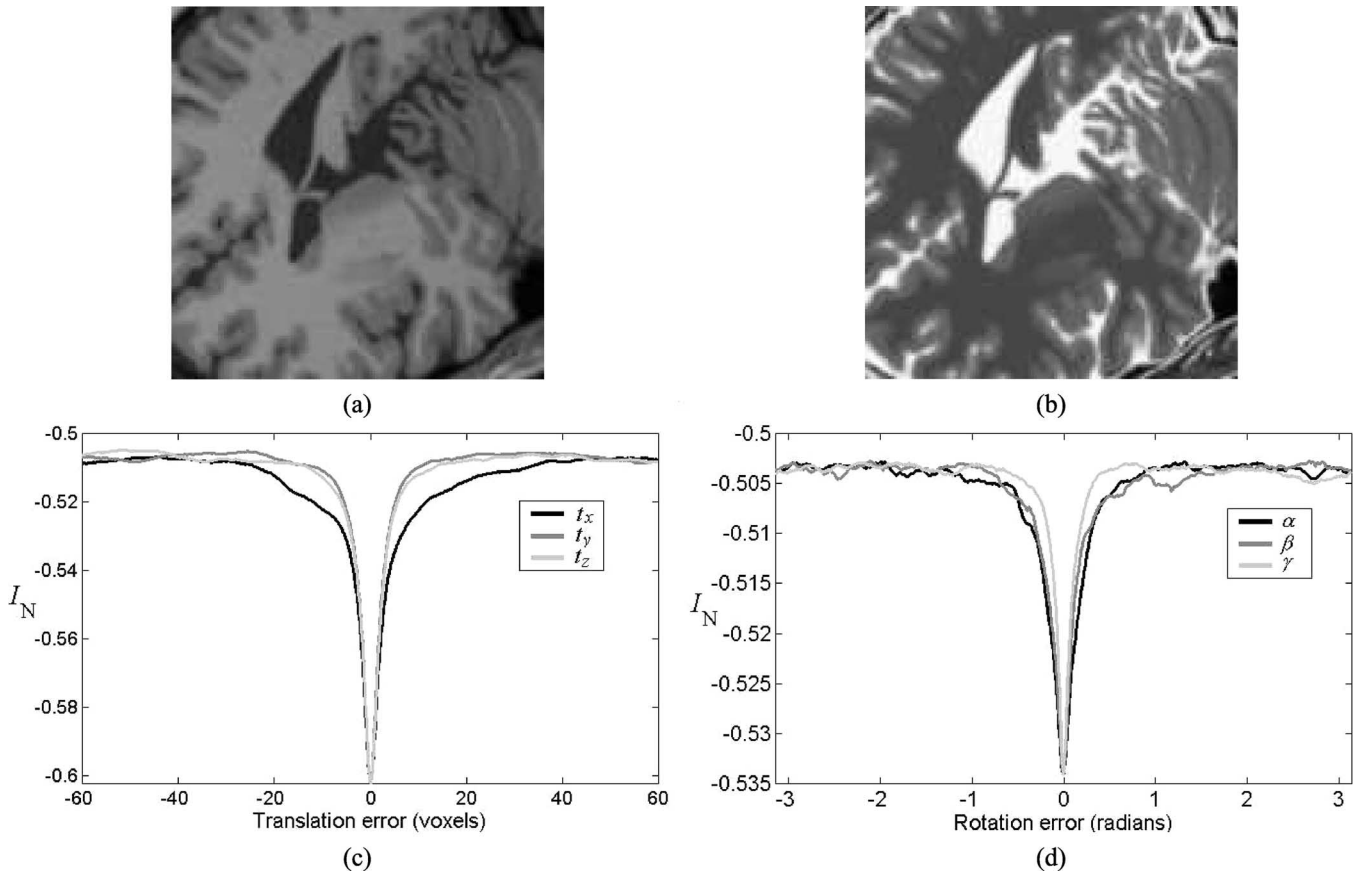

Fig. 3. (a) Slice from T1 MRI head volume. (b) Corresponding T2 image. (c) Normalized mutual information as a function of translation errors. (d) Normalized mutual information as a function of rotation errors.

A. Modifications to the PSO Algorithm

The basic PSO algorithm can be enhanced in a variety of ways. For example, when updating $\mathbf{x}_i$, the best position in a neighborhood of $\mathbf{x}_i$, denoted as $\mathbf{p}'_i$, can be used in updating the velocity instead of the global best position; that is, $\mathbf{p}'_i$ is substituted for $\mathbf{g}$ in (5) [31]. Neighborhoods of $\mathbf{x}_i$ are defined as $\{\mathbf{x}_j \,|\, j \neq i, \|\mathbf{x}_j - \mathbf{x}_i\| < \tau(\mathbf{x}_i)\}$, where $\|\cdot\|$ is some distance measure and the threshold $\tau(\mathbf{x}_i)$ is a function of the maximum distance of all particles from $\mathbf{x}_i$, (denoted as $d_{\max}$), and the iteration t [31]. An example of a neighborhood rule is that a particle $\mathbf{x}_j$, $j \neq i$, is a neighbor of $\mathbf{x}_i$ if [31]

$$\frac{\|\mathbf{x}_i - \mathbf{x}_j\|}{d_{\max}} < \frac{(c_1 t + c_2 t)}{T}. \tag{7}$$

Here, and c_1 and c_2 are positive constants. Thus, there are theoretically as many distinct neighborhoods as particles.

Another modification to PSO is to add ES/GA operators, such as mutation and crossover [25], [32]. In this hybrid PSO, after particle positions have been updated, particles are selected, in pairs, for crossover with probability p_c. For each pair, two child particles are generated by a crossover rule and replace the parents, keeping the population size constant. One such crossover rule for parents $\mathbf{x}_i$ and $\mathbf{x}_j$, $i \neq j$, is [32]

$$\begin{aligned} \mathbf{x}'_i &= p\mathbf{x}_i + (1-p)\mathbf{x}_j \\ \mathbf{x}'_j &= p\mathbf{x}_j + (1-p)\mathbf{x}_i \\ p &\sim \mathrm{UNIF}(0,1). \end{aligned} \tag{8}$$

The velocities $\mathbf{v}_i$ and $\mathbf{v}_j$ of the children can be updated from the velocities of the parents as follows [32]:

$$\mathbf{v}'_i = \mathbf{v}_i V, \quad \mathbf{v}'_j = \mathbf{v}_j V, \quad V = \frac{(\mathbf{v}_i + \mathbf{v}_j)}{\|\mathbf{v}_i + \mathbf{v}_j\|}. \tag{9}$$

The probabilities p in (8) can differ for each parameter of $\mathbf{x}$. Another modification to the hybrid PSO algorithm just described is to group the particles into subpopulations [32]. Any clustering method, such as k-means clustering, can be used to determine the subpopulations. In this case, in addition to p_c, a probability p_{sc} is specified to denote the probability of intrasubpopulation crossover. Crossover among different subpopulations occurs with probability $1 - p_{sc}$ [32].

Another modification designed to control the movement of the $\mathbf{x}_i$ is introduction of a *constriction coefficient* χ [26]. By modeling the velocity update (5) as a deterministic system, a generalized particle swarm model was proposed to control both convergence and "explosive" particle movements [25]. A simple constriction model for velocity update is given as [25]

$$\begin{aligned} \mathbf{v}_i(t) = \chi[&\mathbf{v}_i(t-1) + \varphi_1 u_1 (\mathbf{p}_i - \mathbf{x}_i(t-1)) \\ &+ \varphi_2 u_2 (\mathbf{g} - \mathbf{x}_i(t-1))] \end{aligned} \tag{10}$$

$$\chi = \frac{2\kappa}{|2 - \varphi - \sqrt{\varphi^2 - 4\varphi}|}$$

$$\varphi = \varphi_1 + \varphi_2, \quad \varphi > 4, \quad \kappa \in [0,1]. \tag{11}$$

B. PSO Approach for Registration Utilizing Initial Position

In a large amount of the PSO literature (and in optimization literature in general), standard test functions (e.g., the Rastrigrin and Griewank functions) are employed for benchmark testing. In these cases, the initial set of parameters $\mathbf{x}_0$ has little importance. However, in many practical applications, there is usually at least some knowledge of the characteristics of $\mathbf{x}^*$ for which $f(\mathbf{x}^*)$ is the global minimum. Users of biomedical image registration systems are generally skilled clinical professionals who have an indication of the correct orientation. These users can choose an accurate initial transformation. Although registration is required due to the complexity of medical images and to human error, registration algorithms can still benefit from an accurate initial guess. Consider the t_x curve in Fig. 1(c). If the initial x axis orientation is only $+15$ voxels from the correct transformation, an optimization algorithm may follow the t_x slope to a misregistration of $+40$ voxels. This situation may also be true of PSO, as $\mathbf{v}_{\max}$ and χ only prevent the $\mathbf{x}_i$ from straying from the region of feasible solutions. However, if the $\mathbf{x}_i$ were drawn back to the user's (well-placed) initial orientation, the particles, while "swarming," may have a higher probability of discovering a region that contains $\mathbf{x}^*$. In other words, in addition to the swarming effect around the global best so far $(\mathbf{g})$ and each particle's recollection of its personal best $(\mathbf{p}_i)$, a third factor, the initial orientation $(\mathbf{x}_{\text{init}})$, can also affect the velocity of each particle. In this case, (5) is modified to become

$$\begin{aligned}\mathbf{v}_i(t) = {} & w(t)\mathbf{v}_i(t-1) + \varphi_1 u_1 \left(\mathbf{p}_i - \mathbf{x}_i(t-1)\right) \\ & + \varphi_2 u_2 \left(\mathbf{g} - \mathbf{x}_i(t-1)\right) + \varphi_3 u_3 \left(\mathbf{x}_{\text{init}} - \mathbf{x}_i(t-1)\right) \end{aligned} \tag{12}$$

where φ_3 is the acceleration constant for the return to the initial orientation. Similarly, (10) can be modified to

$$\begin{aligned}\mathbf{v}_i(t) = {} & \chi \left[\mathbf{v}_i(t-1) + \varphi_1 u_1 \left(\mathbf{p}_i - \mathbf{x}_i(t-1)\right)\right. \\ & + \varphi_2 u_2 \left(\mathbf{g} - \mathbf{x}_i(t-1)\right) \\ & \left. + \varphi_3 u_3 \left(\mathbf{x}_{\text{init}} - \mathbf{x}_i(t-1)\right)\right] \end{aligned} \tag{13}$$

$$\chi = \frac{2\kappa}{\left|2 - \varphi - \sqrt{\varphi^2 - 4\varphi}\right|}$$

$$\varphi = \varphi_1 + \varphi_2 + \varphi_3, \quad \varphi > 4, \quad \kappa \in [0, 1]. \tag{14}$$

The technique is illustrated in Fig. 4, where a contour plot of normalized mutual information for 2-D US to 3-D histological registration is shown. The current $\mathbf{g}$, actually a local minimum, is shown exerting attraction on the other particles, but the effect of the initial position steers some of the particles in the direction of the global optimum.

Although stochastic and evolutionary global optimization techniques, including PSO, can generally discover the promising region, or "basin of attraction" of $f(\mathbf{x})$ where $\mathbf{x}^*$ is located, they generally exhibit slow convergence to $\mathbf{x}^*$. As indicated earlier, the complexity of similarity metric computation necessitates fast convergence. Therefore, a local method is applied to the best point in the promising region found by the PSO. Although many local techniques exist, Powell's direction set algorithm was chosen. It does not require derivative computation, and has been shown to be robust and efficient. It is widely used in registration applications [3], [15].

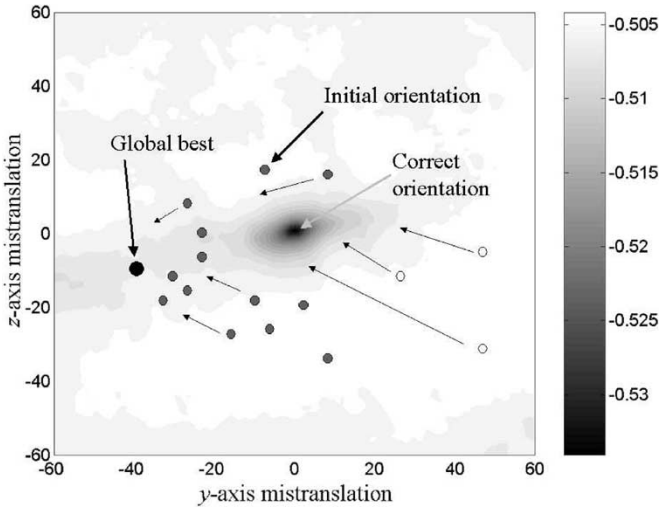

Fig. 4. Illustration of the proposed PSO algorithm utilizing initial position. The contours represent the normalized mutual information landscape of 2-D US to 3-D histological registration. The current global best position $\mathbf{g}$ is in the area of a local minimum. Although the particles begin to swarm around $\mathbf{g}$, some of the particles (white circles) are veered slightly toward the point representing the initial orientation, and would eventually find the "basin of attraction" for the global minimum.

In initial experiments with PSO registration (described below in the Results section), it was found that the PSO-ES hybrid and PSO incorporating the constriction coefficient produced the highest percentage of correct registrations among all PSO techniques tested. Therefore, the modification utilizing the initial orientation was applied to those methods, resulting in three algorithms.

1) **Hybrid PSO with crossover**: This algorithm utilizes the crossover operators for positions and velocities, as described by (8) and (9) [32]. However, for normal velocity updates, (12) is used. Convergence criteria is $T_{\text{NoImprove}} = 20$ iterations in which there is no improvement in $f(\mathbf{g})$, or attaining the maximum number of iterations T. After convergence, Powell's local optimization method is applied to the best point in the swarm. The resulting point contains the parameters of the final registration transformation: $\mathbf{x}^* = [t_x^*\ t_y^*\ t_z^*\ \alpha^*\ \beta^*\ \gamma^*]$. The acceleration constants φ_1 and φ_2 in (12) are set to a fixed value of 2.0. φ_3 is also initially set to 2.0, but decreases to 1.0 during the search according to: $\varphi_3 = \varphi_3 - 1.0/T_{\text{NoImprove}}$. Dynamically changing φ_3 in this way decreases the effect of $\mathbf{x}_0$ over time.
2) **Hybrid PSO with crossover and subpopulations**: This algorithm is the same as that described above, except that five subpopulations, initially determined with k-means clustering, were used. Additionally, after convergence (same criteria as above), Powell's method is applied to the best points in each subpopulation, and the resulting best point is output as the parameter vector of the final registration transformation.
3) **PSO with constriction coefficient and relaxed convergence criteria**: This algorithm is the most "controlled" of the three techniques. A "loose" local optimization with Powell's method (convergence is detected when $f(\mathbf{x})$

TABLE I
VOLUMES AND IMAGES USED IN REGISTRATION EXPERIMENTS

Volume			2D Image		
Modality	Size (voxels)	Comments	Modality	Size (pixels)	Comments
Histological (Abdomen) Volume 1	312×212×149	Downsampled by 4. New voxel size: 1.2 mm	Ultrasound	133×133	Simulated, downsampled by 4.
Histological (Head) Volume 2	174×204×149	Downsampled by 4. New voxel size: 1.2 mm	CT	133×155	Downsampled by 4.
T1 MRI, (Head) Volume 3	181×217×181	Normal, 3% Noise. New voxel size: 1 mm	T2 MRI	128×128	3% noise

changes by less than 0.05) is applied to $\mathbf{x}_0$, resulting in $\mathbf{x}'_0$. Then, particles are generated around $\mathbf{x}'_0$. PSO with constriction factor χ is applied, and the velocities are updated according to (13). Convergence criteria are more relaxed. If in some iteration $f(\mathbf{x}_i) < f(\mathbf{g})$, then $\mathbf{g}$ is set to $\mathbf{x}_i$, but if $\|\mathbf{x}_i - \mathbf{g}\| < \varepsilon$, then the iteration is still considered to be a nonimproving iteration. Convergence is faster, as the iteration counter is not reset to zero for improving points very close to $\mathbf{g}$. Powell's local optimization is applied to $\mathbf{g}$ after convergence (a function value change of less than 0.005).

IV. METHODS

To test the performance of the PSO techniques in biomedical image registration, several registration experiments were performed using a variety of these algorithms.

A. Data

Experiments consisted in registering single slice biomedical images to 3-D volumes. There were three 3-D volumes, and four 2-D images to be registered with each volume. The volume/image modalities, sizes, and properties are shown in Table I. An abdominal volume (henceforth, denoted as volume 1) was obtained through the NLM-NIH Visible Human Project, and consists of histological sections from a deceased female. Corresponding ultrasound images are realistic B-mode simulations generated from physical parameters of ultrasound scattering: the density, size (cross section), and regularity of the placement of the scatterers in tissue [33]. The image and volume are shown in Fig. 1(a) and (b). A head volume (volume 2) was also obtained through the Visible Human Project, as were corresponding CT images registered to this volume [Fig. 2(a) and (b)]. In both cases, the images and volumes were downsampled by 4 and interpolated to reduce the memory and storage requirements. A realistic simulated T1 MRI volume of a normal brain (volume 3) was obtained from the BrainWeb database at McGill University [34], [35]. A section of the T1 volume and corresponding T2 image are shown in Fig. 3(a) and (b). The purpose of this simulator is to provide researchers with ground truth data for image analysis techniques and algorithms.

B. Initial Orientations

Local optimization methods (gradient descent, Powell's method, simplex techniques) have proven very successful in image registration, provided that the initial transformation is reasonably close to the correct orientation [17]. They are also susceptible to premature convergence to local minima, especially for nonsmooth functions. In global optimization techniques, such as evolutionary paradigms and particle swarm optimization, such minima may dominate the search. However, as the global optimum is also a local optimum, the wider search capabilities of the global techniques facilitates one of the local optima eventually emerging as the global optimum.

In the registration experiments, each 2-D image was oriented at 10, 15, 20, and 25 voxels from ground truth translation. In the context of the volumes that were used in this study, these distances are relatively "far" from the correct orientation. Thus, the registrations are considered to be difficult. For each distance, ten rotational orientations were applied, ranging from 5° to 45° out of plane of the correct transformation. For each 2-D image, distance, and orientation, ten trials were performed. A different random number seed, chosen in advance for repeatability, was used for each trial.

C. Registration Controls

Normalized mutual information was computed by (4) using 64 histogram bins, which generally produces a smooth density approximation while retaining intensity features [9]. Because translation and rotation parameters are real-valued, interpolation of voxel intensity values is required, as voxel positions fall on an isotropic grid. Partial volume interpolation [36], in which the intensity histogram is updated using weighted intensities of neighboring voxels, was used in this study, as this method was found to reduce transients and artifacts in the similarity metric function [36].

D. Optimization Techniques

Eight PSO techniques were used to perform the registrations. For comparison, registrations were also performed on seven ES techniques. The similarity metric in all experiments was normalized mutual information. Results were compared on the following merit measures:

1) Accuracy, as measured by the ratio of correct registrations to all registrations. A registration is considered to be cor-

rect if the Euclidean distance from the ground truth translation ($[t_{x0}, t_{y0}, t_{z0}]$) and final translation ($[t'_x, t'_y, t'_z]$) is less than 2 voxels, and if the maximum absolute value of the three rotation errors is less than 2°. These values have been found to be good indicators of registration quality.

2) Efficiency, as measured by the mean number of function evaluations for correct registrations for each 2-D image registered to a 3-D volume.

The ES algorithms used for optimization are now described. For all algorithms, the population size was $N = 35$ (an empirically good value). Specific details of the algorithms are indicated by citations of the appropriate literature. In the following discussion, let $\mathbf{x}_{i,d}$ denote the dth dimension parameter of $\mathbf{x}_i$. Additionally, for all algorithms, including ES, Powell's method was applied for local optimization after convergence criteria for the global optimization were reached.

1) **ES1**: A variant of a generational ES with linear crossover [37], [38]. For each mutation, only one parameter (t_x, t_y, t_z, α, β, γ), chosen at random, was perturbed. The maximum number of generations was set to 100, with convergence criteria being nonimprovement of the cost function for 20 generations. After convergence, the best $\mathbf{x}$ was kept for a new "restart" generation, while the other individuals were reinitialized. The maximum number of restart generations was set to 10, with convergence criteria being nonimprovement of the cost function for three restart generations. The mutation step sizes σ were updated according to [38]

$$\begin{aligned} \sigma'_d &= \sigma_d \exp\left(N(0, \tau_0)\right) \\ \mathbf{x}'_d &= \mathbf{x}_d + \varepsilon, \quad \text{where } \varepsilon \sim \mathrm{N}(0, \sigma_d) \end{aligned} \tag{15}$$

with $\tau_0 = N^{-1/2}$.

2) **ES2**: The same as ES1, except that all parameters are perturbed during mutation [22].
3) **ES3**: The same as ES1, but with multiple-parents crossover [39]. Up to $D = 6$ parents are possible.
4) **ES4**: The same as ES1, except that the σ_d were updated by self-adaptation (crossover and mutation). That is, the σ_d control parameters were coded in the gene [38].
5) **ES5**: The same as ES4, except that the σ_d were updated with Rechenberg's 1/5 success rule [38].
6) **ES6**: Steady-state replacement with self-adapting control parameters [38]. The convergence criterion was 20 nonimproving generations, up to a maximum of 100. The probability of mutation p_m was updated with a lognormal random number [38]: $p_m = p_m \exp(\tau_0 N(0,1) + \tau_1 N(0,1))$, with learning rates $\tau_0 = 0.7$ and $\tau_1 = 0.3$.
7) **ES7**: The same as ES6, but with control parameters updated with Rechenberg's 1/5 success rule.

The following PSO techniques were tested. The total number of particles was set to $N = 35$.

1) **PSO1** (Basic PSO algorithm): For translations, the maximum velocity was set to 20, and for rotations, to π. These values were empirically found to give good results in many trials. The convergence criterion was 20 nonimproving iterations, up to a maximum of $T = 100$ iterations. The inertial weights were adapted according to (6) with $w_{\max} = 0.98$ and $w_{\min} = 0.4$. φ_1 and φ_2 were set to 2.0 [31]. For t_x, t_y, and t_z, the maximum velocity was set to 20.0 voxels, and the maximum velocity for α, β, and γ was set to π radians.
2) **PSO2** (PSO with neighborhood operations [31]): The control parameters were set as in PSO1. In (7), $c_1 = 1$ and $c_2 = 0$.
3) **PSO3** (Hybrid PSO with crossover [32]): The empirically good crossover probability $p_c = 0.4$ was used.
4) **PSO4** (Hybrid PSO with crossover and subpopulations [32]): The probability of crossover, p_c, was set to 0.4, and the probability of intrasubpopulation crossover p_{sc} was set to 0.3. There were five subpopulations, initially determined with k-means clustering.
5) **PSO5**: Hybrid PSO with crossover, similar to PSO3, but with velocities updated according to (12), as described in Section III-B, with $p_c = 0.4$, $\varphi_1 = 2.0$, $\varphi_2 = 2.0$, and φ_3 initially set to 2.0, and decreased in each iteration as $\varphi_3 = \varphi_3 - 1.0/T_{\text{NoImprove}}$.
6) **PSO6**: This algorithm implements the hybrid PSO with crossover and subpopulations. It is similar to PSO4, except that velocities are updated according to (13). The crossover probabilities are the same as in PSO4, with $\varphi_1 = 2.0$, $\varphi_2 = 2.0$, and φ_3 initially set to 2.0, and dynamically decreased, as in PSO5.
7) **PSO7**: Basic PSO with constriction coefficient. The values in (11) were set as follows: $\kappa = 1.0$, $\varphi_1 = 2.8$, $\varphi_2 = 1.3$ [25], [40]. Therefore, $\chi = 0.7298$. PSO7 may be considered as a special case of PSO1 with fixed coefficients.
8) **PSO8**: This is the PSO with constriction coefficient and relaxed convergence criteria, described in Section III-B. The values in (14) were set as follows: $\kappa = 1.0$, $\varphi_1 = 2.1$, $\varphi_2 = 1.2$, $\varphi_3 = 0.8$. These constants were chosen to maintain the constriction coefficient $\chi = 0.7298$. φ_3 was set lower than the other acceleration constants to prevent excessive influence from the initial point. A new point with an improved function value does not cause the improvement counter to be reset if the Euclidean distance between its x, y, and z positions and those of $\mathbf{g}$ is less than 1.5, and if the rotational change is less than 0.0698 radians (about 4°).

V. Results

A. Accuracy

The ratios of correct registrations for the PSO and ES techniques are shown in Fig. 5(a) and (b), respectively. Fig. 5(a) shows that addition of the constriction factor and the term for $\mathbf{x}_0$ (PSO8) improved registration accuracy. In general, the basic PSO technique (PSO1) was the worse performer among PSO methods. Hybridization with the crossover operator also improved accuracy. The three overall best performers [with hybridization (PSO5), hybridization and subpopulations (PSO6), and constriction coefficient (PSO8)] all utilized $\mathbf{x}_0$. Among the ES methods, three generational methods (ES1, ES2, and ES3) had the highest registration accuracy. These methods approximate multistart algorithms, as, after a number of nonimproving generations, all but the best orientation are replaced. In image

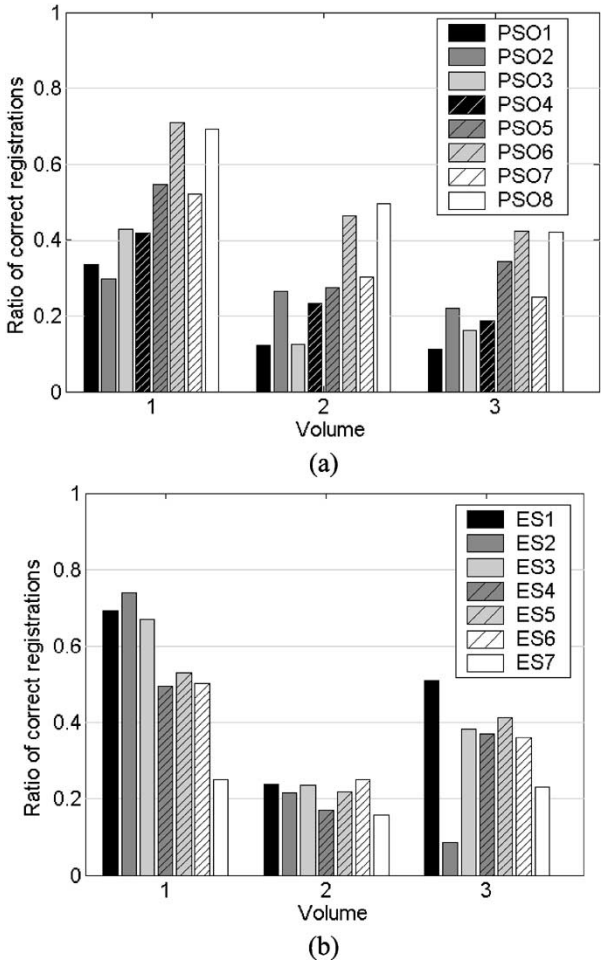

Fig. 5. Registration accuracy, as measured by the ratio of correct registrations for (a) PSO techniques and (b) ES methods.

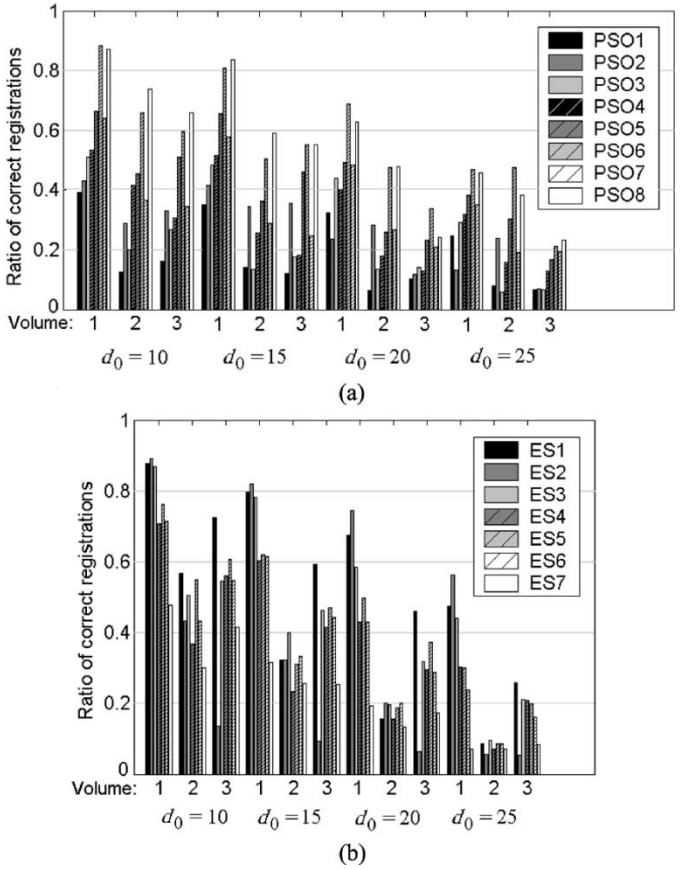

Fig. 6. Registration accuracy as a function of the distance d_0 from ground truth. d_0 is measured using only translations. (a) PSO methods and (b) ES methods.

registration, this added diversity appears to greatly increase the number of correct registrations.

The effect of the initial Euclidean distance d_0 (using t_x, t_y, and t_z) from ground truth was examined, and the results for each volume for PSO and ES are shown in Fig. 6(a) and (b), respectively. As expected, there is a general trend of decreasing accuracy the further $\mathbf{x}_0$ is placed from ground truth. The US-histology registrations, which had the overall best results for all techniques, also exhibited high accuracy for all distances (but also decreasing with distance). An interesting result is that PSO6 (hybrid with subpopulations and $\mathbf{x}_0$ term) and PSO8 (constriction coefficient and $\mathbf{x}_0$ term) were less sensitive to d_0 than the other PSO methods. For the ES methods, the three best performers also had the highest accuracy for all distances. The trend again underscores that registration is sensitive to $\mathbf{x}_0$, even when global optimization is used.

B. Efficiency

In biomedical image registration, accuracy is the primary concern, as it useless to converge quickly to incorrect transformations. However, because of the complexity of evaluating similarity metrics, efficiency is extremely important. The mean numbers of function evaluations for each initial distance (d_0) are given in Table II, and the mean computation times (900 MHz Pentium processor), in seconds, are shown in Table III. Because global and local optimization are both utilized in registration, these values also include evaluations from local optimizations. As expected, PSO6, which performs local optimization on all the local best positions, required the highest number of evaluations. From Table II, the three best ES methods had similar efficiencies. The efficiency for the PSO methods compares favorably with ES efficiency, but with higher standard deviation, indicating that, while some trials converged quickly, others required many function evaluations. PSO5 had the fastest mean convergence of the best methods (but with high standard deviation). PSO8, which was the most accurate among PSO methods, converged slightly more slowly than the best ES algorithm (ES1).

VI. Discussion

The proposed modifications to the velocity update (12), (13) were designed specifically for image registration. As shown in Figs. 1–3(c) and (d), similarity metric functions are often characterized by many local optima. Although the constriction coefficient prevents the particles from straying out of the space of feasible solutions, the particles have a greater probability of being drawn out of local optima by the additional $\mathbf{x}_0$ term. Although this term improved registration accuracy, in other applications, there may be no prior knowledge of the location of the global optimum. Therefore, in some cases, PSO8 may prevent particles from moving toward the global optimum, and only the

TABLE II
MEAN NUMBER OF FUNCTION EVALUATIONS (× 1000) FOR ES AND PSO TECHNIQUES. THE THREE MOST ACCURATE ES AND PSO TECHNIQUES ARE SHOWN IN BOLDFACE

Volume	Algorithm	$d_0 = 10$	$d_0 = 15$	$d_0 = 20$	$d_0 = 25$
US – Hist.	**ES1**	**2.26±20.394**	**2.154±0.294**	**2.382±0.353**	**2.341±0.423**
	ES2	**2.128±0.383**	**2.299±0.414**	**2.204±0.388**	**2.333±0.360**
	ES3	**2.169±0.390**	**2.171±0.366**	**2.272±0.496**	**2.245±0.418**
	ES4	1.131±0.229	1.094±0.158	1.135±0.211	1.159±0.143
	ES5	1.123±0.209	1.216±0.204	1.269±0.194	1.158±0.206
	ES6	0.816±0.155	0.831±0.148	0.835±0.113	0.842±0.071
	ES7	0.821±0.154	0.817±0.172	0.760±0.146	0.852±0.473
	PSO1	1.889±0.195	1.824±0.191	1.801±0.201	1.995±0.000
	PSO2	1.294±0.235	1.337±0.272	1.397±0.278	1.501±0.271
	PSO3	2.754±0.999	3.202±0.828	2.415±0.888	3.121±0.800
	PSO4	2.543±0.544	2.351±0.472	2.429±0.561	1.970±0.281
	PSO5	**1.802±0.546**	**1.689±0.450**	**2.125±0.706**	**2.379±0.776**
	PSO6	**3.467±0.683**	**3.765±0.849**	**3.502±0.801**	**3.650±0.629**
	PSO7	3.674±0.048	3.660±0.015	3.698±0.139	3.550±0.523
	PSO8	**2.367±0.601**	**2.449±0.705**	**2.674±0.641**	**2.736±0.687**
CT – Hist.	**ES1**	**2.138±0.299**	**2.111±0.432**	**2.251±0.495**	**2.353±0.276**
	ES2	**2.095±0.379**	**2.152±0.293**	**2.136±0.355**	**2.264±0.406**
	ES3	**2.050±0.250**	**2.277±0.241**	**2.159±0.248**	**2.229±0.234**
	ES4	1.111±0.225	1.094±0.164	0.971±0.200	1.189±0.164
	ES5	1.065±0.156	1.111±0.147	1.102±0.276	1.251±0.401
	ES6	0.773±0.088	0.721±0.099	0.787±0.124	0.738±0.072
	ES7	0.801±0.122	0.833±0.102	0.670±0.029	0.809±0.210
	PSO1	1.843±0.170	1.768±0.119	1.776±0.188	1.957±0.305
	PSO2	1.336±0.272	1.215±0.251	1.307±0.232	1.351±0.215
	PSO3	2.461±1.209	2.330±1.206	2.528±1.359	3.127±1.036
	PSO4	2.423±0.582	2.463±0.406	2.601±0.907	2.669±0.480
	PSO5	**1.876±0.841**	**1.795±0.681**	**1.873±0.608**	**1.310±0.172**
	PSO6	**3.390±0.461**	**3.532±0.515**	**3.627±0.543**	**3.513±0.521**
	PSO7	2.919±0.801	2.832±0.876	2.990±0.813	2.710±0.726
	PSO8	**2.236±0.539**	**2.238±0.693**	**2.347±0.556**	**1.997±0.438**
T1– T2 MRI	**ES1**	**2.207±0.281**	**2.490±0.496**	**2.473±0.497**	**2.503±0.357**
	ES2	**1.680±0.216**	**2.174±0.535**	**2.167±0.000**	**0.000±0.000**
	ES3	**2.384±0.322**	**2.330±0.459**	**2.271±0.202**	**2.518±0.506**
	ES4	1.332±0.219	1.243±0.221	1.297±0.255	1.313±0.359
	ES5	1.352±0.216	1.342±0.365	1.333±0.298	1.523±0.021
	ES6	0.957±0.148	0.986±0.169	0.982±0.139	0.908±0.157
	ES7	0.945±0.209	0.969±0.174	1.080±0.235	0.903±0.389
	PSO1	1.953±0.167	1.996±0.267	1.981±0.071	2.281±0.481
	PSO2	1.371±0.340	1.404±0.291	1.635±0.359	1.487±0.283
	PSO3	2.854±1.129	3.032±1.111	3.010±1.005	3.124±0.970
	PSO4	2.444±0.378	2.313±0.285	2.673±1.023	2.305±0.451
	PSO5	**1.938±0.721**	**1.897±0.643**	**2.205±0.723**	**2.387±0.767**
	PSO6	**3.982±1.023**	**3.818±0.868**	**3.818±0.808**	**3.681±0.938**
	PSO7	3.569±0.600	3.803±0.170	3.680±0.061	3.686±0.065
	PSO8	**2.428±0.775**	**2.434±0.729**	**2.375±0.714**	**2.594±0.863**

$\mathbf{p}_i$ and $\mathbf{g}$ should be used for velocity update. If a feasible region, wherein the correct transformation plausibly lies, cannot be identified, then other PSO techniques, such as the use of crossover and subpopulations (PSO6), is recommended.

In addition, it may be argued that the use of local optimization within the PSO and ES imply a weakness of global methods. However, local optimization is, in itself, often inadequate for finding the correct registration. This fact is demonstrated in Table IV, where the ratio of correct registrations is shown using only Powell's method for local optimization. By comparing these values to those shown in Fig. 6, global optimization clearly improved accuracy for all d_0.

For the ES methods, the relatively good performance of the generational approaches suggests the following.

1) Diversity, maintained by replacement of most of the population in every generation, is important in avoiding entrapment in local optima.
2) The "restart generations," in which all but the best individual are replaced, also facilitates adequate exploration of the search space.
3) However, if a good position is identified, the individual should be "slightly" mutated (only one parameter is mutated in ES1), encouraging intensive searching around promising regions.

TABLE III
MEAN TIME (IN SECONDS) FOR ES AND PSO TECHNIQUES. THE THREE MOST ACCURATE ES AND PSO TECHNIQUES ARE SHOWN IN BOLDFACE

Volume	Algorithm	$d_0 = 10$	$d_0 = 15$	$d_0 = 20$	$d_0 = 25$
US – Hist.	**ES1**	**244.69±98.26**	**252.72±90.25**	**246.65±94.16**	**229.32±99.82**
	ES2	**192.16±34.66**	**197.36±33.90**	**203.54±36.17**	**210.96±32.10**
	ES3	**163.68±48.71**	**170.35±56.75**	**175.53±50.26**	**179.38±61.18**
	ES4	99.46±20.14	97.63±23.22	97.40±20.88	99.48±17.34
	ES5	99.20±24.05	98.87±23.49	100.77±22.54	100.46±24.02
	ES6	74.82±12.00	75.48±12.89	77.95±12.85	76.74±10.95
	ES7	69.49±14.74	72.16±11.89	70.43±14.62	68.08±15.95
	PSO1	119.12±10.68	120.95±16.38	114.47±14.92	122.83±21.77
	PSO2	183.58±34.85	188.48±38.33	193.67±34.58	206.79±36.70
	PSO3	352.21±140.41	370.83±135.32	371.04±136.94	386.88±138.88
	PSO4	335.12±69.49	322.62±68.59	322.08±76.78	312.72±73.54
	PSO5	**246.02±77.67**	**248.41±76.57**	**304.61±99.73**	**339.13±101.51**
	PSO6	**362.43±115.65**	**359.55±105.68**	**355.12±101.42**	**352.24±116.54**
	PSO7	519.15±11.15	521.34±10.32	519.37±15.83	515.92±36.70
	PSO8	**213.84±55.95**	**216.32±61.91**	**222.78±57.30**	**251.81±61.93**
CT – Hist.	**ES1**	**310.39±93.34**	**338.80±98.64**	**306.52±86.13**	**346.00±77.80**
	ES2	**227.53±39.58**	**238.06±33.99**	**241.43±36.20**	**251.56±45.60**
	ES3	**311.43±76.17**	**302.94±72.49**	**298.14±73.71**	**299.57±92.22**
	ES4	138.61±66.82	146.41±70.55	142.65±63.78	166.00±59.56
	ES5	132.62±65.89	145.24±70.58	146.31±66.69	187.57±42.75
	ES6	103.27±41.33	103.73±41.90	111.21±45.31	117.00±46.61
	ES7	95.94±38.81	99.30±44.45	110.81±43.84	113.78±38.74
	PSO1	158.65±18.61	157.16±16.73	154.43±19.73	166.85±31.54
	PSO2	204.15±40.15	195.04±30.01	192.68±29.97	201.42±40.25
	PSO3	360.62±172.36	395.20±161.06	415.14±175.74	429.14±179.77
	PSO4	371.04±72.45	367.14±65.75	368.18±77.15	374.36±63.38
	PSO5	**250.30±89.83**	**285.33±94.49**	**253.67±91.19**	**265.09±105.02**
	PSO6	**505.68±105.54**	**727.53±251.04**	**501.14±96.14**	**497.45±125.28**
	PSO7	443.75±191.03	422.95±190.34	421.26±188.09	393.65±199.81
	PSO8	**229.54±92.70**	**207.90±71.84**	**233.30±99.50**	**196.06±58.73**
T1– T2 MRI	**ES1**	**294.86±72.55**	**299.73±87.05**	**296.88±83.46**	**291.93±81.23**
	ES2	**187.92±41.20**	**217.88±43.79**	**184.00±35.36**	**272.20±116.05**
	ES3	**264.80±75.98**	**256.47±78.11**	**273.59±75.23**	**253.12±72.46**
	ES4	103.40±21.19	102.56±19.03	107.17±21.05	104.45±20.85
	ES5	104.47±18.74	106.79±22.66	106.31±21.97	101.40±22.01
	ES6	176.00±893.67	78.14±17.91	75.84±23.22	77.29±15.86
	ES7	70.64±15.48	69.98±17.36	67.57±16.73	69.08±16.75
	PSO1	160.87±31.60	159.30±27.47	172.32±49.10	182.73±60.22
	PSO2	191.23±30.97	198.00±37.42	196.76±28.97	218.45±29.09
	PSO3	339.29±137.67	389.00±137.50	419.57±130.00	427.00±138.79
	PSO4	314.26±68.11	343.19±99.11	319.44±51.10	325.65±81.07
	PSO5	**252.51±81.69**	**256.91±76.14**	**274.26±82.76**	**309.11±80.89**
	PSO6	**504.50±128.75**	**527.85±133.17**	**548.52±148.67**	**546.42±134.55**
	PSO7	449.16±109.38	494.11±15.05	501.93±17.79	498.00±17.76
	PSO8	**253.05±112.89**	**262.41±110.23**	**271.82±107.06**	**278.67±102.66**

TABLE IV
RATIO OF CORRECT REGISTRATIONS USING ONLY POWELL'S LOCAL OPTIMIZATION

Volume	$d_0 = 10$	$d_0 = 15$	$d_0 = 20$	$d_0 = 25$
1 (abdomen histological)	0.35	0.36	0.18	0
2 (head histological)	0	0.33	0.11	0
3 (T1 MRI)	0.30	0.30	0.10	0.05

For the PSO methods:

1) Some knowledge of the correct orientation can greatly benefit the search.
2) Both the $\mathbf{x}_0$ term and the constriction coefficient prevent the search from straying too far from the global optimum.
3) Hybridization with ES operators appear to improve accuracy by diversifying particle locations.
4) Convergence criteria during the global search can be relaxed, as local optimization can find the global optimum if a particle is sufficiently close to it. Additionally, the convergence of PSO8 can be potentially be improved by eliminating the initial Powell optimization.

The PSO method (PSO8) outperformed all ES methods for CT-histological registrations. For the US-histological

registrations, accuracy was nearly identical for the three best PSO and ES methods. In the MRI registrations, ES1 had a slight advantage over the best PSO methods. However, the PSO methods were noticeably more accurate than the other ES techniques.

Both accuracy and efficiency of the PSO methods can be improved by additional modifications, such as better swarm initialization [41]. However, in the scope of the current study, it was shown that incorporation of the initial position into the velocity update equation, by itself, greatly increased registration accuracy.

Finally, registration performance is also highly dependent on the similarity metric. Although normalized mutual information was utilized in the present study, other metrics may be more conducive to optimization [2], [42], and may further enhance the correctness, accuracy, and efficiency of the PSO (and other) approaches.

VII. Conclusion

A new adaptation of particle swarm optimization specifically designed for biomedical image registration was proposed in this paper. An additional term containing the initial user-specified orientation to the velocity update equation draws the search away from local optima far from the correct registration. Although registration success is then more dependent on the initial position, in actual practice, a good guess is highly likely. Registration performance for the PSO methods is also improved by hybridization with crossover operators and with constriction coefficients. Experimental results for PSO compare very favorably with ES techniques, both in terms of accuracy and efficiency. PSO performance was enhanced by addition of evolutionary operators, indicating that hybrid global optimization merits further exploration. In fact, the results presented in this paper not only demonstrate the efficacy of using PSO for image registration, but also generally support the use of stochastic global optimization for biomedical image registration. Both evolutionary techniques and PSO are inherently parallel, and computation times can be greatly improved by utilizing either distributed- or shared-memory architectures. Incorporation of multiresolution strategies may also improve performance. Although comparisons must be made with other global and local optimization paradigms and similarity metrics, and the methods must also be adapted for nonlinear alignment, particle swarm optimization has been shown to be promising for optimization in biomedical image registration.

Acknowledgment

The authors thank the faculty and staff of the BrainWeb project at McGill University, Montreal, QC, Canada, for making their MRI simulator available. Thanks are also given to the National Library of Medicine for the visible human data. The authors gratefully acknowledge J. H. Brown, R. Lile, and Dr. M. Kantardzic for use of computer facilities. Finally, thanks are given to the anonymous reviewers for many helpful and constructive suggestions.

References

[1] J. V. Hajnal, D. L. G. Hill, and D. J. Hawkes, "View of the future," in *Medical Image Registration*, J. V. Hajnal, D. L. G. Hill, and D. J. Hawkes, Eds. Boca Raton, FL: CRC, 2001.

[2] D. L. G. Hill, P. G. Batchelor, M. Holden, and D. J. Hawkes, "Medical image registration," *Phys. Med. Biol.*, vol. 46, pp. R1–R45, 2001.

[3] J. B. A. Maintz and M. A. Viergever, "A survey of medical image registration," *Med. Image Anal.*, vol. 2, pp. 1–37, 1998.

[4] U. Pietrzyk, "Registration of MRI and PET images for clinical applications," in *Medical Image Registration*, J. V. Hajnal, D. L. G. Hill, and D. J. Hawkes, Eds. Boca Raton, FL: CRC, 2001.

[5] M. Jenkinson and S. Smith, "The role of registration in functional magnetic resonance imaging," in *Medical Image Registration*, J. V. Hajnal, D. L. G. Hill, and D. J. Hawkes, Eds. Boca Raton, FL: CRC, 2001.

[6] L. Brown, "A survey of image registration techniques," *ACM Comput. Surv.*, vol. 24, pp. 325–376, 1992.

[7] D. L. G. Hill and P. Batchelor, "Registration methodology: concepts and algorithms," in *Medical Image Registration*, J. V. Hajnal, D. L. G. Hill, and D. J. Hawkes, Eds. Boca Raton, FL: CRC, 2001.

[8] A. Roche, X. Pennec, G. Malandain, and N. Ayache, "Rigid registration of 3-D ultrasound with MR images: A new approach combining intensity and gradient information," *IEEE Trans. Med. Imag.*, vol. 20, pp. 1038–1049, Oct. 2001.

[9] F. Maes, A. Collignon, D. Vandermeulen, G. Marchal, and P. Suetens, "Multimodality image registration by maximization of mutual information," *IEEE Trans. Med. Imag.*, vol. 16, pp. 187–198, Apr. 1997.

[10] W. M. Wells III, P. Viola, H. Atsumi, S. Nakajima, and R. Kikinis, "Multi-modal volume registration by maximization of mutual information," *Med. Image Anal.*, vol. 1, pp. 35–51, 1996.

[11] C. Studholme, D. L. G. Hill, and D. Hawkes, "An overlap invariant entropy measure of 3D medical image alignment," *Pattern Recognit.*, vol. 32, pp. 71–86, 1999.

[12] K. McLeish, D. L. G. Hill, D. Atkinson, J. M. Blackall, and R. Razavi, "A study of the motion and deformation of the heart due to respiration," *IEEE Trans. Med. Imag.*, vol. 21, pp. 1142–1150, Sept. 2002.

[13] B. Likar and F. Pernuš, "A hierarchical approach to elastic registration based on mutual information," *Image Vis. Comput.*, vol. 19, pp. 33–44, 2001.

[14] M. Wierzbicki and T. M. Peters, "Determining epicardial surface motion using elastic registration: Toward virtual reality guidance of minimally invasive cardiac interventions," in *Lecture Notes in Computer Science*, Proc. MICCAI—2978, pp. 697–704.

[15] J. P. W. Pluim, J. B. A. Maintz, and M. A. Viergever, "Image registration by maximization of combined mutual information and gradient information," *IEEE Trans. Med. Imag.*, vol. 19, pp. 809–814, Aug. 2000.

[16] J. L. Bernon, V. Boudousq, J. F. Rohmer, M. Fourcade, M. Zanca, M. Rossi, and D. Mariano-Goulart, "A comparative study of Powell's and downhill simplex algorithms for a fast multimodal surface matching in brain imaging," *Comput. Med. Imaging Graph.*, vol. 25, pp. 287–297, 2001.

[17] F. Maes, D. Vandermeulen, and P. Suetens, "Comparative evaluation of multiresolution optimization strategies for multimodality image registration by maximization of mutual information," *Med. Image Anal.*, vol. 3, pp. 373–386, 1999.

[18] J. P. W. Pluim, J. B. A. Maintz, and M. A. Viergever, "Mutual information matching in multiresolution contexts," *Image Vis. Comput.*, vol. 19, no. 1–2, pp. 45–52, 2001.

[19] M. Jenkinson and S. Smith, "A global optimization method for robust affine registration of brain images," *Med. Image Anal.*, vol. 5, pp. 143–156, 2001.

[20] G. K. Matsopoulos, N. A. Mouravliansky, K. K. Delibasis, and K. S. Nikita, "Automatic retinal image registration scheme using global optimization techniques," *IEEE Trans. Inform. Technol. Biomed.*, vol. 3, pp. 47–60, Mar. 1999.

[21] J. M. Rouet, J. J. Jacq, and C. Roux, "Genetic algorithms for a robust 3-D MR-CT registration," *IEEE Trans. Inform. Technol. Biomed.*, vol. 4, pp. 126–136, June 2000.

[22] R. He and P. A. Narayana, "Global optimization of mutual information: application to three-dimensional retrospective registration of magnetic resonance images," *Comput. Med. Imaging Graph.*, vol. 26, no. 4, pp. 277–292, 2002.

[23] M. P. Wachowiak and A. S. Elmaghraby, "The continuous tabu search as an optimizer for 2D-to-3D biomedical image registration," in *Lecture Notes in Computer Science*, W. Niessen and M. Viergever, Eds. New York: Springer-Verlag, 2001, Proc. MICCAI 2001—2208, pp. 1273–1274.

[24] J. Kennedy and R. C. Eberhart, "Particle swarm optimization," in *Proc. IEEE Int. Conf. Neural Networks*, vol. 4, Perth, Australia, Dec. 1995, pp. 1942–1948.
[25] ——, *Swarm Intelligence*. San Mateo, Ca: Morgan Kaufman, 2001.
[26] M. Clerc and J. Kennedy, "The particle swarm—explosion, stability, and convergence in a multidimensional complex space," *IEEE Trans. Evol. Comput.*, vol. 6, pp. 58–73, Feb. 2002.
[27] Particle Swarm Central. [Online]. Available: http://www.particleswarm.net/papers.html.
[28] V. Tandon, H. El-Mounayri, and H. Kishawy, "NC end milling optimization using evolutionary computation," *Int. J. Mach. Tools Manuf.*, vol. 42, pp. 595–605, 2002.
[29] A. R. Cockshott and B. E. Hartman, "Improving the fermentation medium for echinocandin B production Part II: Particle swarm optimization," *Process Biochem.*, vol. 36, pp. 661–669, 2001.
[30] M. A. Abido, "Optimal power flow using particle swarm optimization," *Elec. Power, Energy Syst.*, vol. 2, pp. 563–571, 2002.
[31] P. N. Suganthan, "Particle swarm optimizer with neighborhood operator," in *Proc. 1999 Congr. Evolutionary Computation*, Washington, DC, July 1999, pp. 1958–1962.
[32] M. Lovbjerg, T. K. Rasmussen, and T. Krink, "Hybrid particles swarm optimizer with breeding and subpopulations," in *Proc. 3rd Genetic Evolutionary Computation Conf.*, San Francisco, CA, 2001, pp. 469–476.
[33] V. M. Narayanan and P. M. Shankar, "Non-Rayleigh statistics of ultrasonic backscattered signals," *IEEE Trans. Ultrason., Ferroelect., Freq. Contr.*, vol. 41, pp. 845–852, Nov. 1994.
[34] R. K.-S. Kwan, A. C. Evans, and G. B. Pike, "MRI simulation-based evaluation of image-processing and classification methods," *IEEE Trans. Med. Imag.*, vol. 18, pp. 1085–1097, Nov. 1999.
[35] D. L. Collins, A. P. Zijdenbos, V. Kollokian, J. G. Sled, N. J. Kabani, C. J. Holmes, and A. C. Evans, "Design and construction of a realistic digital brain phantom," *IEEE Trans. Med. Imag.*, vol. 17, pp. 463–468, June 1998.
[36] J. P. W. Pluim, J. B. A. Maintz, and M. A. Viergever, "Interpolation artefacts in mutual information-based image registration," *Comput. Vis. Image Understand.*, vol. 77, pp. 211–232, 2000.
[37] P. Schroeter, J. M. Vesin, T. Lanenberger, and R. Meuli, "Robust parameter estimation of intensity distributions for brain magnetic resonance images," *IEEE Trans. Med. Imag.*, vol. 17, no. 2, pp. 172–186, 1998.
[38] A. E. Eiben, R. Hinterding, and Z. Michalewicz, "Parameter control in evolutionary algorithms," *IEEE Trans. Evol. Comput.*, vol. 3, pp. 124–141, July 1999.
[39] A. E. Eiben and A. Schippers, "On evolutionary exploration and exploitation," *Fundamenta Informaticae*, vol. 35, pp. 35–50, 1998.
[40] A. Carlisle and G. Dozier, "An off-the-shelf PSO," in *Proc. PSO Workshop, IUPUI*, Indianapolis, IN, Apr. 2001.
[41] K. E. Parsopoulos and M. N. Vrahatis, "Initializing the particle swarm optimizer using the nonlinear simplex method," in *Advances in Intelligent Systems, Fuzzy Systems, Evolutionary Computation*, A. Grmela and N. E. Mastorakis, Eds. Athens, Greece: WSEAS Press, 2002, pp. 216–221.
[42] M. P. Wachowiak, R. Smolíková, G. D. Tourassi, and A. S. Elmaghraby, "Similarity metrics based on nonadditive entropies for 2D-3D multimodal biomedical image registration," *Proc. SPIE*, pp. 1090–1100, 2003.

Mark P. Wachowiak (S'99–M'02) received the Ph.D. degree from the Department of Computer Engineering and Computer Science, University of Louisville, Louisville, KY, in 2002.

He is a Postdoctoral Fellow at the Robarts Research Institute, London, ON, Canada. His research interests include medical imaging, biomedical engineering, computational biology, scientific computing and visualization, applied mathematics, high-performance computing, and mathematical modeling of physiological systems.

Dr. Wachowiak is a Member of the IEEE Engineering in Medicine and Biology Society and the Society for Industrial and Applied Mathematics (SIAM).

Renata Smolíková (S'01–M'02) received the Ph.D. degree in mathematics from Palacky University, Olomouc, Czech Republic, in 1999 and the Ph.D. degree in computer science and engineering from the University of Louisville, Louisville, KY, in 2002.

She was an Assistant Professor with the Department of Mathematics, University of Ostrava, Czech Republic. She is currently a Postdoctoral Fellow in the Imaging Laboratories, Robarts Research Institute, London, ON, Canada. Her research interests include medical image registration, ultrasound backscatter analysis, neural networks, and applied mathematics.

Dr. Smolíková is a Member of the Society for Industrial and Applied Mathematics (SIAM) and the IEEE Engineering in Medicine and Biology Society.

Yufeng Zheng received the Ph.D. degree from the Tianjin University, Tianjin, China, in 1997.

He is currently with the University of Louisville, Louisville, KY, as a Postdoctoral Research Associate. His research interests focus on digital image processing, including image registration and fusion, noise reduction, image restoration and enhancement, edge detection, segmentation, and pattern recognition.

Jacek M. Zurada (M'82–SM'83–F'96) is the S.T. Fife Alumni Professor of Electrical and Computer Engineering, University of Louisville, Louisville, KY. He is the coeditor of *Knowledge-Based Neurocomputing* (Cambridge, MA: MIT Press, 2000), *Computational Intelligence: Imitating Life* (Piscataway, NJ: IEEE Press, 1994), and the author of *Introduction to Artificial Neural Systems* (Boston, MA: PWS-Kent, 1992). He is the author or coauthor of more than 200 journal and conference papers in the area of neural networks and VLSI circuits.

Dr. Zurada has been the Editor-in-Chief of IEEE TRANSACTIONS ON NEURAL NETWORKS since 1998. He was the recipient of the 2001 University of Louisville President's Distinguished Service Award for Service to the Profession. He is currently the President of IEEE Neural Networks Society in 2004–2005. In March 2003, he was conferred the Title of the Professor by the President of Poland, A. Kwasniewski.

Adel S. Elmaghraby (S'78–M'81–SM'85) is a Professor and Chair of the Computer Engineering and Computer Science Department and the Director of the Multimedia Research Laboratory, University of Louisville, Louisville, KY. He has also held appointments at Carnegie Mellon University, Pittsburgh, PA, and the University of Wisconsin—Madison. His research is in intelligent multimedia systems, neural networks, biomedical computing, visualization, and simulation. He serves on several editorial boards, and is a technical reviewer.

Dr. Elmaghraby has been recognized for his achievements by several professional organizations, including a Golden Core Membership Award by the IEEE Computer Society.